Fluorescent Marangoni Flows under Quasi-Steady Conditions

Cesar Usma, Sandrine Mariot, Claire Goldmann, Matthieu Roché, Anniina Salonen, Guillaume Tresset

Fluorescent Marangoni Flows under Quasi-Steady Conditions

Cesar L. Usma,[†] Sandrine Mariot,[†] Claire Goldmann,[†] Matthieu Roché,[*,‡] Anniina Salonen,[*,†] and Guillaume Tresset[*,†]

[†]*Université Paris-Saclay, CNRS, Laboratoire de Physique des Solides, 91405 Orsay, France*

[‡]*Université de Paris, CNRS, Matière et Systèmes Complexes, 75013 Paris, France*

E-mail: matthieu.roche@u-paris.fr; anniina.salonen@universite-paris-saclay.fr; guillaume.tresset@universite-paris-saclay.fr

Abstract

Marangoni flow is amongst the most intriguing effects in complex fluids and interfacial science. We report here on a fluorescent surfactant that enables to monitor Marangoni flows under quasi-steady conditions, without the need of invasive tracers. The Marangoni zone is clearly visible and its dynamics can be quantitatively probed both at the air-water interface and within the bulk. In particular, we show that the Marangoni zone exhibits unexpected dependencies with the container size and water depth with the pyrene-tailed surfactant. Additionally, recirculation flows are evidenced by fluorescence near the bottom of the container. This fluorescent probe may find other useful applications in deciphering the complexity of the ubiquitous Marangoni effect.

Introduction

The Marangoni effect is a spectacular manifestation of the interfacial forces driven by surfactants at the air-water interface. It stems from the gradients of surface tension arising from the

inhomogeneity of the surfactant density across the air-water interface, which subsequently induce the motion of both fluids.[1] A vast literature is dedicated to the Marangoni effect as it plays an important role in many natural and industrial processes such as clean drying processes for the fabrication of integrated circuits and liquid crystals displays.[2] Arthropods such as the rove beetles *Microvelia* and *Stenus* slide over the water surface by expelling an organic compound that lowers the surface tension to the rear.[3] Microfabricated, bioinspired devices dispensing autonomously alcohol or other chemicals based on Marangoni propulsion were reported (e.g.[4]). Marangoni flows also ensure the stability of foams by resisting the drainage of the thin films separating bubbles and thereby extend their lifetime.[5]

One way for investigating the Marangoni effect is to deposit a drop of surfactant solution on thin films.[6,7] Following this approach, Fallest and coworkers monitored the transient spreading of fluorescent phospholipids on a thin layer of glycerin.[8] However, the transient nature of the induced flow makes it difficult to elucidate the underlying physics. Roché and coworkers[9] developed an axisymmetric setup allowing them to study Marangoni flows under quasi-steady conditions, a configuration similar to the one used in the past to gain insights on typical velocities and stability of Marangoni flows.[10–14] By continuously injecting a surfactant solution containing tracers made of oil droplets on the surface of a water bath, they observed a transparent zone – i.e., depleted in tracers –, with a finite size that is related to the surfactant solubility. The same transparent zone, hereafter referred to as Marangoni zone, was also reported when the Marangoni flow was confined laterally producing an inertial surface jet.[15,16] In these flows, partition of surfactants between the air-water interface and bulk water is sensitive to both advection induced by the Marangoni stress and surface-volume exchanges.[15] Bandi *et al.* identified two regimes:[17] At low injected surfactant concentrations, the Marangoni flow is driven by the adsorbed surfactants at the air-water interface, while at high injected surfactant concentrations, the flow is dominated by the surfactants dissolved into the bulk. Beyond the fundamental motivation for a better understanding of the Marangoni effect, experimental setups can be utilized to estimate the critical micelle con-

centration of surfactant through a single measurement,[9,15] in contrast with existing methods that require to measure the surface tension as a function of the surfactant concentration.

In the previously mentioned studies with continuous injection of a surfactant solution, surface flows were either monitored with tracers that could affect the flow properties, or by laser doppler velocimetry, and fluorescent phospholipids could not be used owing to their insolubility in the injected solution. In other words, surfactants were never probed directly under quasi-steady conditions, which limited so far the information obtained on the Marangoni effect, notably regarding the fate of surfactants in the bulk. Here, we present the use of a fluorescent, pyrene-based amphiphilic molecule that gives a direct signature of the Marangoni flows in an axisymmetric setup. We investigate in particular the effects related to the bulk through the container size and water depth, and we monitor the flow patterns occurring at and below the air-water interface with unprecedented details.

Experimental

Surfactant synthesis

The synthesis of pyrene ammonium surfactant (Fig. 1) is adapted from a protocol first reported elsewhere.[18] All reactants are purchased from Merck (Saint Quentin Fallavier, France). ^{1}H-NMR spectra are obtained with a Bruker AVANCE 300 (300 MHz) Fourier transform NMR spectrometer with chemical shifts reported in parts per million (ppm) relative to tetramethylsilane. Splitting patterns are reported as s (singlet), d (doublet), t (triplet), and multiplet (m).

Synthesis of 2-Bromoethyl 4-(1-pyrenyl)butanoate (1)

Briefly, in a 500-mL round-bottomed flask, 10.8 g of pyrenebutyric acid (37.5 mmol) are dissolved in 100 mL of dry dichloromethane, followed by 5.32 mL of bromoethanol (75 mmol) and 2.29 g of 4-dimethylaminopyridine (DMAP) (18.7 mmol). 11.56 g of N,N'-

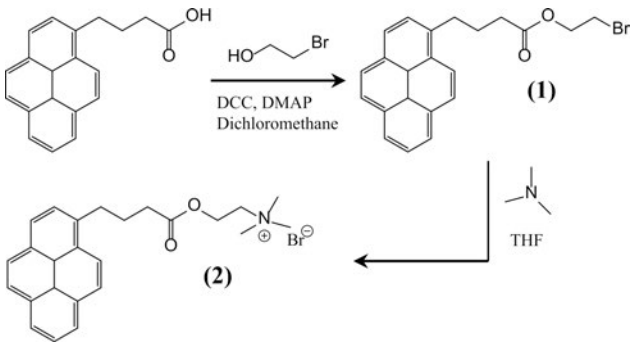

Figure 1: Reaction scheme for the synthesis of pyrene ammonium surfactant.

dicyclohexylcarbodiimide (56 mmol) are added slowly thanks to a funnel. After 24 h, the reaction medium is filtered, the filtrate is washed with water, dried with $MgSO_4$, filtered and evaporated to give 19.7 g of a beige solid. Purification on a silica column yields 11.7 g of a white-greenish solid.

^{1}H NMR ($CDCl_3$) : 2.24 ppm, m, 2H ; 2.53 ppm, t, 2H ; 3.45 ppm, t, 2H ; 3.53 ppm, t, 2H ; 4.43 ppm, t, 2H ; 7.88-8.34 ppm, m, 9H.

Synthesis of 2-[4-(1-Pyrenyl)butanoyloxy]ethyltrimethylammonium bromide (2)

11.7 g of 2-bromoethyl 4-(1-pyrenyl)butanoate (30 mmol) are dissolved in 50 mL of THF and 10 mL of trimethylamine (50% in H_2O, 75 mmol) are added dropwise at room temperature. The reaction is left to stir for one week and filtered. The precipitate is dried under vacuum at room temperature and stored in a closed, dark flask while the filtrate is evaporated under vacuum at 25 °C and put again with trimethylamine (same proportion) for one week. The procedure is repeated until a satisfactory amount of precipitate is obtained, namely here, 12.36 g.

^{1}H NMR, DMSO: 2.07 ppm, m, 2H ; 2.53 ppm, m, 2H ; 3.12 ppm, m, 9H ; 3.34 ppm, m, 2H ; 3.66 ppm, m, 2 H ; 4.47 ppm, m, 2H ; 7.95-8.42 ppm, m, 9H.

Physicochemical characterizations

Fluorescence and absorbance spectroscopy

The fluorescence spectra are measured using a spectrofluorometer Fluoromax 4 from Horiba. Fluorescence emission spectra of a number of surfactant solutions with concentrations between 0.5 μM and 1.5 mM are recorded from 350 to 600 nm using an excitation wavelength of 345 nm. All measurements are performed at room temperature (23 °C). The UV absorption measurements are carried out at room temperature using a spectrophotometer Genesys 50 from Thermo Fischer Scientific, at wavelengths between 250 and 400 nm.

Surface tension measurement

The surface tension is measured with an Ez-Pi + tensiometer from Kibron. The principle of the measurement is based on the Du Noüy – Padday technique. A DyneProbe is placed at the liquid surface and then pulled out. The tearing force related to the surface tension is measured thanks to a sensor with an accuracy of 0.01 mN.m^{-1}, calibrated with ultrapure water. The surfactant samples are placed in a Teflon cup and the measurements are carried out at room temperature (23 °C). The reported values for each surfactant concentration represent the average of at least three experiments. After each measurement the Teflon cup is thoroughly rinsed with tap water followed by rinsing with ultrapure water and the probe is flamed.

In order to determine the minimal area per surfactant molecule at the air-water interface $A_{\min}$, the surface tension measurements are used to calculate the maximum surface excess concentration of surfactant $\Gamma_{\max}$, by applying the Gibbs adsorption:

$$\Gamma_{\max} = -\frac{1}{nRT}\left(\frac{\partial \Upsilon}{\partial \ln C}\right) \tag{1}$$

where R is the gas constant, T the temperature, Υ the surface tension, and C the surfactant concentration. $n = 1$ for non-ionic surfactants, and $n = 2$ for 1:1 ionic surfactants in the

absence of added polyelectrolyte as is the case in our study. The slope $\partial\Upsilon/\partial \ln C$ is estimated in the vicinity of the CMC, where its absolute value is maximal. The minimal area occupied by a single surfactant molecule in nm^2 is then given by:

$$A_{\min} = \frac{10^{18}}{\Gamma_{\max} N_A} \tag{2}$$

with N_A the Avogadro constant.

Setup

A pyrene ammonium surfactant solution at 2 mM is continuously deposited at a constant flow rate Q on top of a bath of ultrapure water (Purelab, Elga Veolia) (Fig. 2a). The surfactant solution is injected with a high-precision syringe pump (KD Scientific Inc.) through an angled stainless steel needle (inner diameter 0.84 mm $\times$ length 38.1 mm, Nordson EFD). For our experiments, the flow rate is varied between 40 $mL.h^{-1}$ and 70 $mL.h^{-1}$. The spreading of surfactant is monitored with fluorescence (Fig. 2b) by illuminating the water surface with a UV lamp (6 W, 365 nm, Bioblock Scientific) and recorded with a camera (Logitech HD 1080p) placed above the injection point. The containers are either a glass Petri dish (diameter 19 cm) or a home-made square plexiglas tank (40×40 cm) unless otherwise stated.

Results

Fluorescence properties of the pyrene ammonium surfactant

Figure 3a illustrates the change of color of surfactant solutions with various concentrations under the same UV light excitation: From purple at 1 μM to light green above 2 mM. Some fluorescence spectra are shown in Fig. 3b with an excitation wavelength of 345 nm. At all surfactant concentrations, we observe finely structured peaks at wavelengths comprised between 370 and 450 nm. For high surfactant concentrations, a broad emission peak – the so-

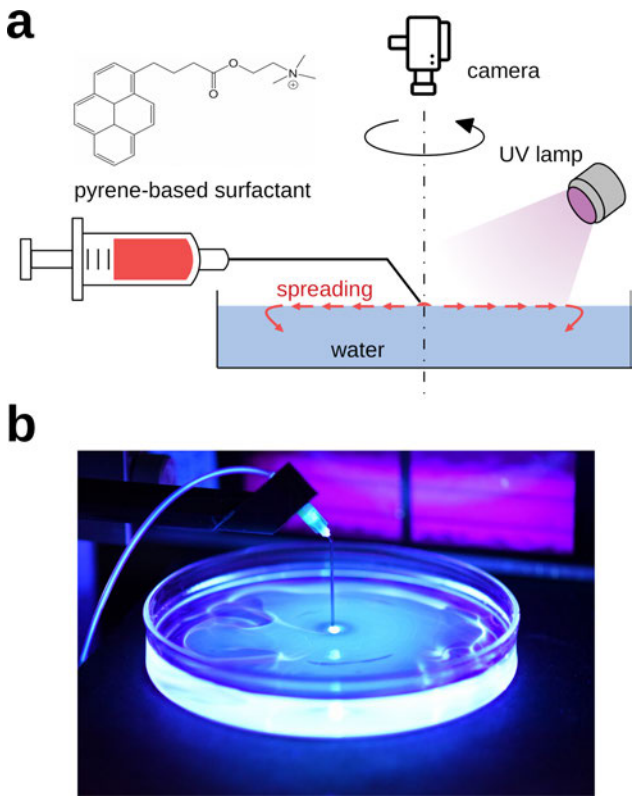

Figure 2: a) Schematic representation of the axisymmetric configuration used in this study. b) Photograph of the actual setup with a glass Petri dish (diameter 9.6 cm).

called excimer peak – appears around 480 nm. It was reported in the fluorescence spectrum of pyrene that the intensity ratio of the first I_1 and third I_3 peaks is a sensitive quantity characterizing the polarity of the environment surrounding the molecule. For example, I_1/I_3 is about 0.6 in hydrocarbon solvent whereas it amounts to 1.8 in water. Figure 3c depicts I_1/I_3 as a function of surfactant concentration. If the ratio remains unchanged at very low concentrations, it clearly drops for concentrations above 0.1 mM, which indicates that the polarity of the environment around each pyrene ring is reduced. This change of environment can be ascribed to the self-association of surfactants into dimers or oligomers through $\pi - \pi$ stacking or hydrophobic interaction.

Additionally, the fact that an excimer peak becomes visible for surfactant concentrations higher than 0.1 mM suggests either a dynamical process or a pre-association of the pyrene groups. In the former case, the incident light excites isolated pyrene groups, which then

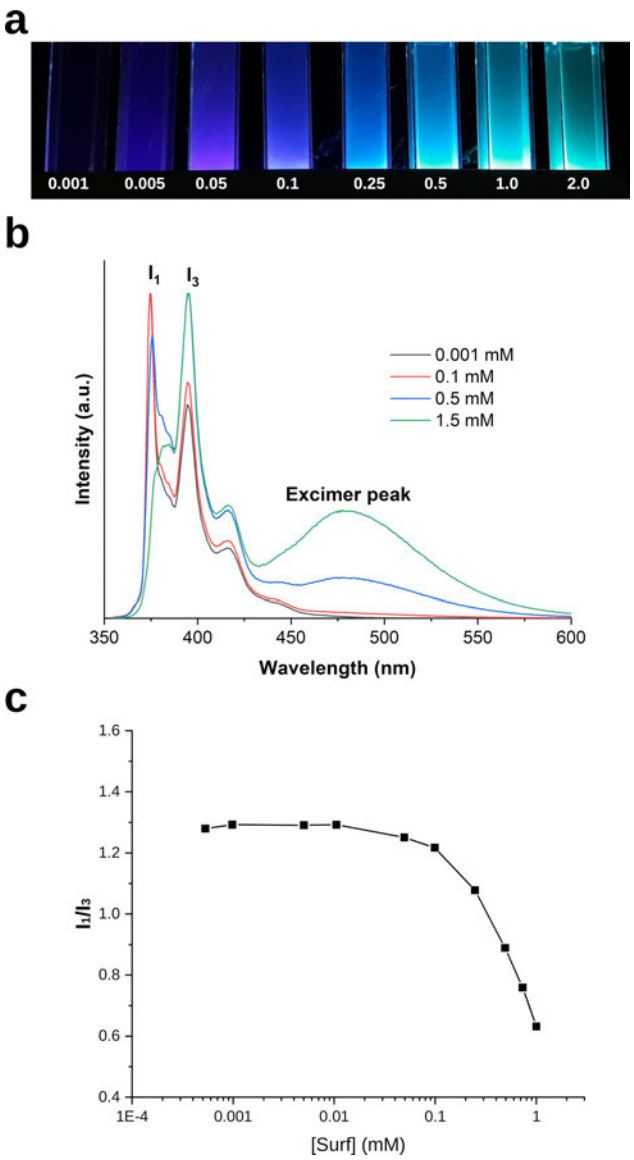

Figure 3: a) Optical image of surfactant solutions at various concentrations under UV light. The figures below the cuvettes are surfactant concentrations in mM. b) Fluorescence emission spectra at various concentrations. c) Ratio of the intensity peaks I_1/I_3 as a function of surfactant concentration. In all cases, the excitation wavelength is set to 345 nm.

diffuse and encounter a ground-state pyrene to form an excimer. Static excimers are formed by direct excitation of pyrene dimers or oligomers. In order to confirm that the excimer peak is due to pre-associated dimers, we can compare the peak-to-valley ratio (P_{A}) from UV absorption spectra obtained at various surfactant concentrations. P_{A} is the ratio of the absorbance of the most intense band of the 0-1 transition ($\sim$ 344 nm) to that of the adjacent

minimum at a shorter wavelength (see Fig. S1a). As depicted by Figure S1b, P_{A} drops for surfactant concentrations larger than 50 μM, which indicates that pre-association of dimers occurs in this range of concentration.

Interfacial properties

Figure 4a shows measurements of the surface tension of surfactant solutions as a function of time. Surface tension decreases steadily with time for surfactant concentrations above 0.25 mM, until stabilization is reached after about 30 min. The evolution of the surface tension with the surfactant concentration measured at equilibrium gives a robust estimate of the critical micelle concentration (CMC). Figure 4b depicts the sharp transition between the regime in which the amount of free or pre-associated surfactants increases linearly with the total surfactant concentration, yielding a gradual decrease of the surface tension, and that in which the excess of surfactants is converted into micellar aggregates in such a way that the surface tension remains unchanged. The obtained CMC is then 0.75 mM and by using Gibbs isotherm, we estimate the minimal occupied area of each surfactant molecule to be 1.42 nm^2. The area is higher than with typical ionic surfactants. This is due to the size of the pyrene tail, which is larger than most surfactant alkane tails and requires more space.[19]

By taking fluorescence and surface tension measurements together, we can propose the following mechanism of association: Surfactant molecules are dissociated until concentrations of 50-100 μM are reached, then they start to be pre-associated in dimeric or oligomeric forms. Above 0.75 mM, micelles are formed in the bulk, and the surface concentration remains constant as evidenced by a constant surface tension. In this interfacial study the surfactant behaves much like classical hydrocarbon surfactants, which makes it an interesting candidate to visualize Marangoni flows. However, we should keep in mind that the pyrene "tail" group is quite different from the fluid hydrocarbon chains. For example in a non-ionic pyrene surfactant studied previously, the interfacial properties were unremarkable, yet even at low concentrations the surfactant formed macrostructures with hexagonal ordering.[20]

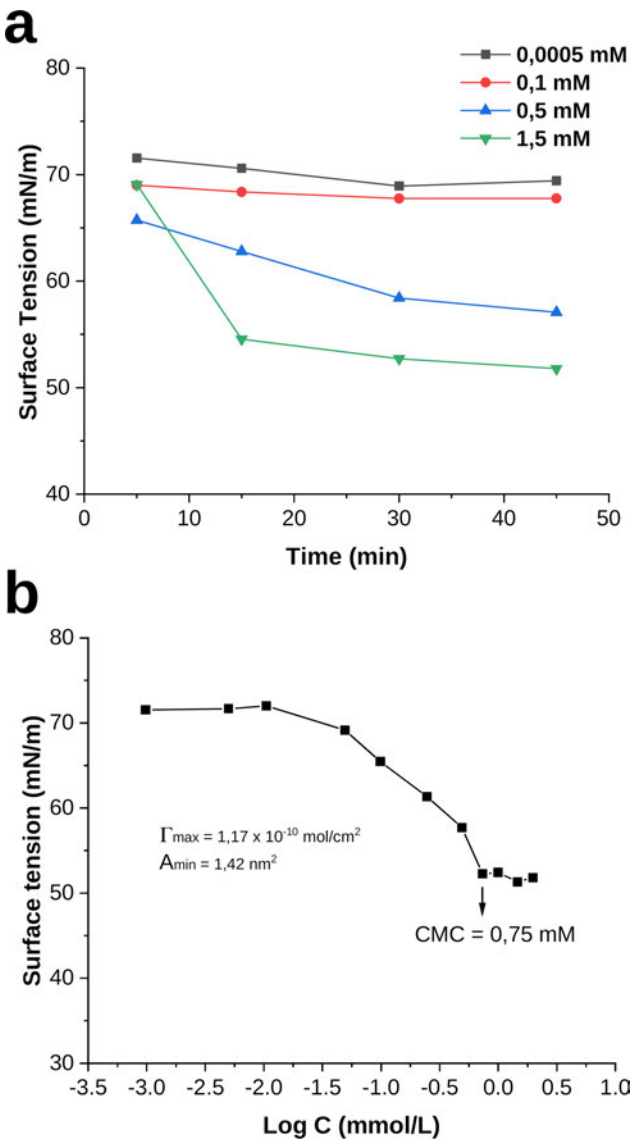

Figure 4: a) Variation of the surface tension of surfactant solutions at various concentrations as a function of time. b) Measurements of the surface tension after equilibration at various concentrations and determination of the critical micelle concentration (CMC).

Expansion of the Marangoni zone with increasing flow rate

We investigate first the effect of the injection flow rate on the surfactant spreading at the air-water interface. As depicted in Fig. 5a, a circular transparent zone appears centered on the injection point in the middle of the images. This Marangoni zone is devoid of fluorescent surfactants because the latter are rapidly spread away through the Marangoni effect. Because the surfactant velocity strongly decreases with the distance from the injection point,[21] sur-

factants accumulate at the edge of the Marangoni zone. Figure 5a shows that the Marangoni zone weakly shrinks after 60 s due to the finite size of the large tank that induces edge effects. Upon the increase of the flow rate Q, the Marangoni zone becomes more extended due to the fact that, under steady state condition, the flux of surfactant diffusing from the Marangoni zone down to the bulk must balance the injection flow rate.[9] The flow rate effect is better evidenced by Fig. 5b that plots the radius of the Marangoni zone R_{M} as a function of time for various flow rates for experiments performed in a Petri dish. After a transient expansion during about 10 s, R_{M} slowly decreases and reaches a fairly stationary value after typically one or two minutes. This behavior is fully consistent with previous observations involving classical hydrocarbon surfactants.[9] By fitting the experimental values taken at 100 s with a power law, i.e., $R_{\mathrm{M}} \propto Q^{\alpha}$, we arrive at a value for α close to 2 (Fig. S3), whereas the mass conservation of surfactants at the air-water interface predicts an exponent $\alpha = 3/4$.[9] The discrepancy can be ascribed to the presence of the fluorescence-emitting pyrene group that induces a lower solubility than that of surfactants with hydrocarbon chain, most likely due to $\pi - \pi$ stacking. In fact, the exponent $\alpha = 3/4$ was established theoretically with a dissolution-dominated surfactant transport, that is, for soluble surfactants at injected concentration well below the CMC. The spreading dynamics of fluorescent surfactants might be rather dominated by adsorption at the air-water interface,[21] explaining in part why the power law in $Q^{3/4}$ fails.

Size effects

In the next series of experiments, we investigate the effect of the water depth on the Marangoni zone. The latter is stable over several minutes regardless of the water depth, whether in a large tank (Fig. 6a) or in a Petri dish (Fig. S2). By plotting R_{M} as a function of the water depth Δ, we can see that the Marangoni zone expands as Δ increases (Fig. 5b), then R_{M} remains constant for water depths $\Delta > \Delta_{\mathrm{c}} \sim 2.5$ cm. In other words, the size of the flow is influenced by the water depth until a critical value Δ_{c} is reached, which is

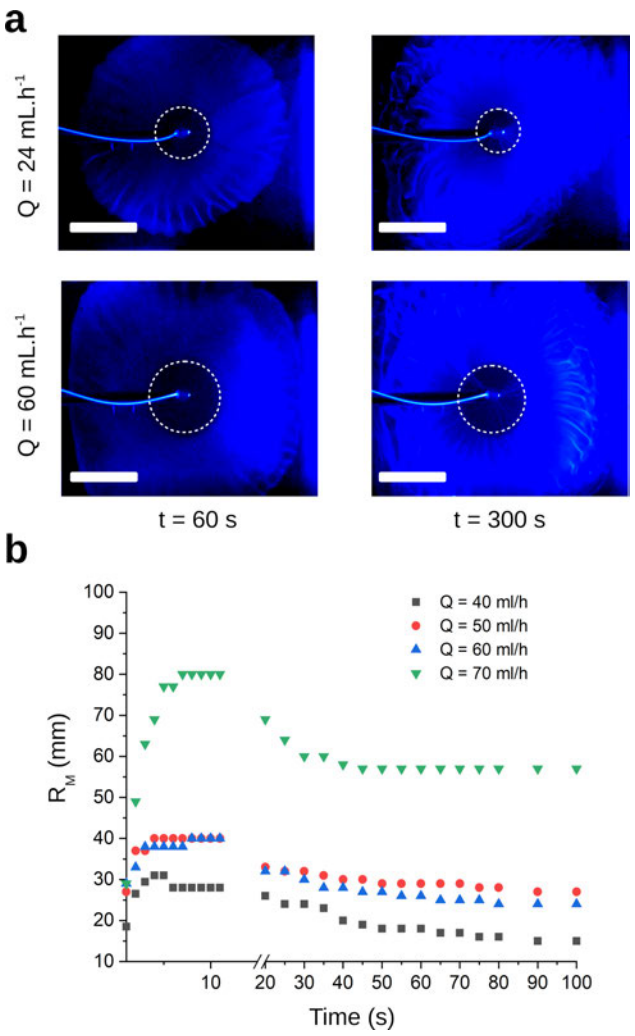

Figure 5: a) Optical images of surfactant spreading under UV illumination with Marangoni zones delimited by dashed circles. Experiments are shown at two surfactant flow rates Q and two time steps. Experiments are performed in a large tank for better visualization. Scale bars are 10 cm. b) Radius of the Marangoni zone R_{M} as a function of time for various surfactant flow rates. Measurements are performed in a Petri dish. Water depth is 1.0 cm.

in sharp contrast with the results obtained for simple surfactants. Another observation is that the average spreading velocity U, experimentally measured by using a polystyrene bead as a tracer, decreases with Δ at fixed flow rate Q (Fig. S4). This is in agreement with the concomitant increase of R_{M}, since, in the regime where the surfactant dynamics is dominated by the dissolved phase, scaling laws predict $U \propto Q^2/R_{\mathrm{M}}^3$.[9] Furthermore, in the same regime, the characteristic length of the viscous boundary layer is expressed by $l_{\mathrm{v}} = \sqrt{\eta R_{\mathrm{M}}/\rho U}$ where η denotes the fluid viscosity and ρ the fluid density. With $\eta = 10^{-3}$ Pa.s, $R_{\mathrm{M}} \sim 10^{-2}$ m,

$\rho \sim 10^3$ kg.m^{-3} and since U is estimated to be 10^{-2} m.s^{-1} (Fig. S4), we arrive at $l_v \sim 10^{-3}$ m, which is one order of magnitude smaller than the typical water depth. Since the spreading dynamics cannot be disturbed by the water depth through the viscous boundary layer, large convection cells must be formed along the vertical direction, transporting surfactants and fluid from the air-water interface to the bottom of the container. Given that R_M is constant for $\Delta > \Delta_c$, the maximal length scale of these convection cells must be of the order of Δ_c, i.e., 2.5 cm in the present case.

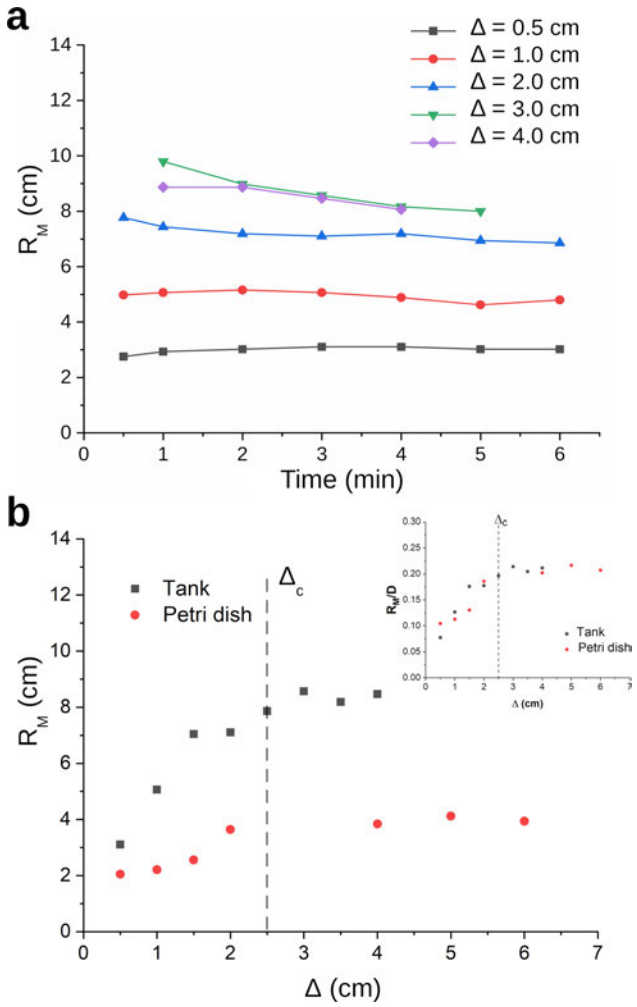

Figure 6: a) Radius of the Marangoni zone R_M as a function of time with various depths in a large tank. b) Radius of the Marangoni zone R_M versus water depth Δ. A Petri dish (red discs) and a large tank (black squares) are used for these spreading experiments. R_M is measured 1 min and 150 s after injection for the experiments in a large tank and Petri dish, respectively. Δ_c is the critical depth. The inset shows the same data normalized to the diameter of the container D. Flow rate is 60 mL.h^{-1} in all cases.

Additionally, the curves of R_M/D versus Δ, where D denotes the diameter of the container, obtained with a Petri dish and a tank collapse (Fig. 6b inset), which means $R_M \propto D$. In both cases, the diameter of the Marangoni zone does not exceed one half of the container size, and yet, the spreading dynamics is seemingly influenced by the container walls. Even though the fluorescence signal is not uniform over the air-water interface (e.g. Fig. 5a), surfactants most likely cover the whole surface, even in the transparent areas where their concentration must be too low to emit detectable light with our conventional camera. Subsequently, the gradient of surface tension driving surfactants out of the Marangoni zone becomes limited by the accumulation of surfactants, even weak, near the container walls.

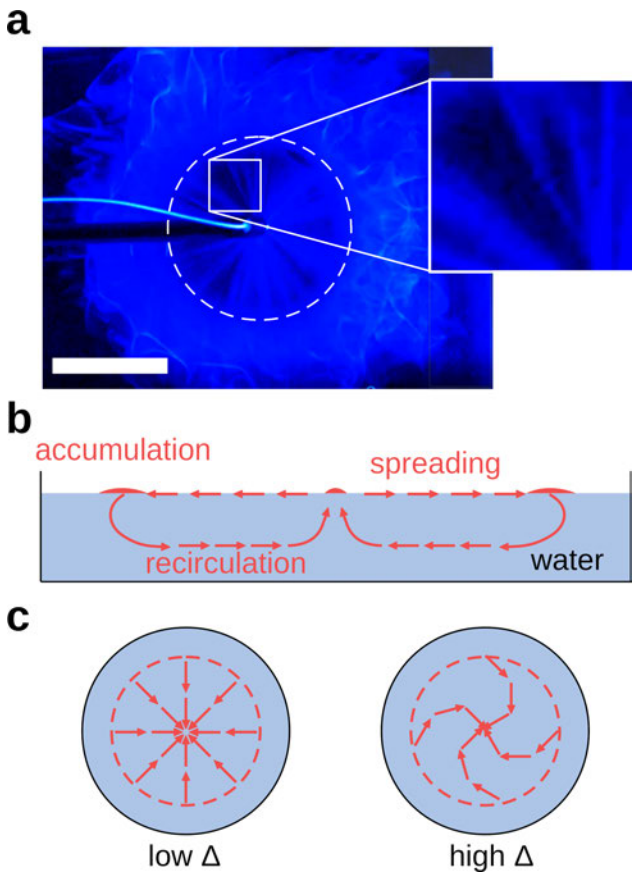

Figure 7: a) Optical image of the surfactant spreading with recirculation flows below the surface. The experimental setup is shown 5 minutes after beginning the injection in a large tank with a water depth of 2 cm. Flow rate is 60 mL.h^{-1}. Scale bar is 10 cm. The inset is a close-up view of surfactant fingers. b) Schematic representation of the surfactant spreading, accumulation at the edge of the Marangoni zone and recirculation below the surface. c) Bottom view of the recirculation flows at low and high water depth Δ.

Recirculation flows

As depicted by Figs. 7a and 7b, surfactants rapidly accumulate near the edge of the Marangoni zone where their velocity vanishes. After a certain time, we observe recirculation flows of surfactants below the surface (Fig. 7a). Recall that the Marangoni zone always remains devoid of fluorescent surfactants, therefore the flows shown in the inset of Fig. 7a are necessarily occurring underneath the air-water interface. Additionally, Movie S1 shows that they gradually appear from the edge of the Marangoni zone toward the injection point, i.e., in the opposite direction of the Marangoni spreading. These flows are better visualized at high Δ values, even though they are observed in all conditions (see Fig. S5). For $\Delta < 3$ cm, after diving below the surface (Fig. 7b), the surfactant flows converge radially towards the center of the Marangoni zone (Fig. 7c, left), which is also the injection point. By contrast, for $\Delta > 3$ cm, the surfactant flows return to the center by forming swirl-like patterns (Fig. 7c, right), which may reveal a link between the recirculation flows and Δ_c. Another interesting feature is that surfactant flows do not recirculate uniformly, they form distinct fingers converging at the injection point (Fig. 7a inset). This phenomenon may stem from an instability driven by the difference of fluid properties between pure water and surfactant flows.

Conclusions

We report a study on Marangoni flows by using a fluorescent surfactant. The Marangoni flows are maintained in quasi-steady state by continuously injecting a surfactant solution on top of a water bath. The fluorescence light emitted by the surfactants allows us to monitor their spatial density in real time, and subsequently the associated flows, without the need of tracers that may change the dynamics. We shed light on unexpected dependencies of the Marangoni zone upon the water depth and the container size, likely related to convection cells and wall effect, respectively. We demonstrate the utility of fluorescent surfactants by revealing flows occurring below the air-water interface. The Marangoni effect is central to

fundamental phenomena in complex fluids physics as well as in industrial processes, and we believe that fluorescent surfactants will contribute to improve our knowledge on this intriguing effect.

Acknowledgement

C. L. U., G. T., A. S. and M. R. acknowledge financial support from the Agence Nationale de la Recherche (contract ANR-17-CE08-0020).

Supporting Information Available

Movie showing the spreading of fluorescent surfactants, UV absorption spectra, radius of the Marangoni zone for various water depths, power law for the radius of the Marangoni zone versus flow rate, average velocity, and optical images of surfactant spreading at various water depths and time steps.

References

(1) Levich, V. G.; Krylov, V. S. Surface-Tension-Driven Phenomena. *Annu. Rev. Fluid Mech.* **1969**, *1*, 293–316.

(2) Leenaars, A. F. M.; Huethorst, J. A. M.; Van Oekel, J. J. Marangoni drying: A new extremely clean drying process. *Langmuir* **1990**, *6*, 1701–1703.

(3) Bush, J. W.; Hu, D. L. Walking on water: Biolocomotion at the Interface. *Annu. Rev. Fluid Mech.* **2006**, *38*, 339–369.

(4) Kwak, B.; Choi, S.; Maeng, J.; Bae, J. Marangoni effect inspired robotic self-propulsion over a water surface using a flow-imbibition-powered microfluidic pump. *Sci. Rep.* **2021**, *11*, 17469.

(5) Cantat, I.; Cohen-Addad, S.; Elias, F.; Graner, F.; Höhler, R.; Pitois, O.; Rouyer, F.; Saint-Jalmes, A. *Foams: Structure and Dynamics*; Oxford University Press: Oxford, 2013.

(6) Gaver, D. P.; Grotberg, J. B. Droplet spreading on a thin viscous film. *J. Fluid Mech.* **1992**, *235*, 399–414.

(7) Lee, K. S.; Starov, V. M. Spreading of surfactant solutions over thin aqueous layers at low concentrations: Influence of solubility. *J. Colloid Interface Sci.* **2009**, *329*, 361–365.

(8) Fallest, D. W.; Lichtenberger, A. M.; Fox, C. J.; Daniels, K. E. Fluorescent visualization of a spreading surfactant. *New J. Phys.* **2010**, *12*, 073029.

(9) Roché, M.; Li, Z.; Griffiths, I. M.; Le Roux, S.; Cantat, I.; Saint-Jalmes, A.; Stone, H. A. Marangoni Flow of Soluble Amphiphiles. *Phys. Rev. Lett.* **2014**, *112*, 208302.

(10) Suciu, D. G.; Smigelschi, O.; Ruckenstein, E. Some Experiments on the Marangoni Effect. *AIChE J.* **1967**, *13*, 1120.

(11) Suciu, D. G.; Smigelschi, O.; Ruckenstein, E. On the Structure of Dissolving Thin Liquid Films. *AIChE J.* **1969**, *15*, 686–689.

(12) Ruckenstein, E.; Smigelschi, O.; Suciu, D. G. A Steady Dissolving Drop Method for Studying the Pure Marangoni Effect. *Chem. Eng. Sci.* **1970**, *25*, 1249–1254.

(13) Suciu, D. G.; Smigelschi, O.; Ruckenstein, E. The Spreading of Liquids on Liquids. *J. Coll. Interface Sci.* **1970**, *33*, 520–528.

(14) Pshenichnikov, A. F.; Yastenko, S. S. Konvektivnaya Diffuziya Ot Sosredotochennogo Istochnika Poverkhnostno-Aktivnogo Veshchestva (Convective Diffusion from a Concentrated Surfactant Source). *Uch. zap. Permsk. Un-ta* **1974**, *316*, 175–181.

(15) Le Roux, S.; Roché, M.; Cantat, I.; Saint-Jalmes, A. Soluble surfactant spreading: How the amphiphilicity sets the Marangoni hydrodynamics. *Phys. Rev. E* **2016**, *93*, 013107.

(16) Tregouet, C.; Saint-Jalmes, A. Stability of a directional Marangoni flow. *Soft Matter* **2020**, *16*, 8933–8939.

(17) Bandi, M. M.; Akella, V. S.; Singh, D. K.; Singh, R. S.; Mandre, S. Hydrodynamic Signatures of Stationary Marangoni-Driven Surfactant Transport. *Phys. Rev. Lett.* **2017**, *119*, 264501.

(18) Chen, J.; Liao, D.; Wang, Y.; Zhou, H.; Li, W.; Yu, C. Real-Time Fluorometric Assay for Acetylcholinesterase Activity and Inhibitor Screening through the Pyrene Probe Monomer–Excimer Transition. *Org. Lett.* **2013**, *15*, 2132–2135.

(19) Xu, Z.; Li, P.; Qiao, W.; Li, Z.; Cheng, L. Effect of aromatic ring in the alkyl chain on surface properties of arylalkyl surfactant solutions. *J. Surfactants Deterg.* **2006**, *9*, 245–248.

(20) Salonen, A.; Knyazev, A.; von Bandel, N.; Degrouard, J.; Langevin, D.; Drenckhan, W. A Novel Pyrene-Based Fluorescing Amphiphile with Unusual Bulk and Interfacial Properties. *ChemPhysChem* **2011**, *12*, 150–160.

(21) Mandre, S. Axisymmetric spreading of surfactant from a point source. *J. Fluid Mech.* **2017**, *832*, 777–792.

Table of Contents (TOC) graphic

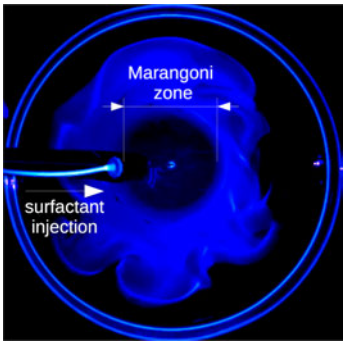

Supporting Information: Fluorescent Marangoni Flows under Quasi-Steady Conditions

Cesar L. Usma,[†] Sandrine Mariot,[†] Claire Goldmann,[†] Matthieu Roché,[*,‡] Anniina Salonen,[*,†] and Guillaume Tresset[*,†]

†*Université Paris-Saclay, CNRS, Laboratoire de Physique des Solides, 91405 Orsay, France*

‡*Université de Paris, CNRS, Matière et Systèmes Complexes, 75013 Paris, France*

E-mail: matthieu.roche@u-paris.fr; anniina.salonen@universite-paris-saclay.fr; guillaume.tresset@universite-paris-saclay.fr

Movie S1

Spreading of fluorescent surfactants observed in a Petri dish with a water depth of 2.0 cm. The flow rate is set to 60 $\mathrm{mL.h^{-1}}$.

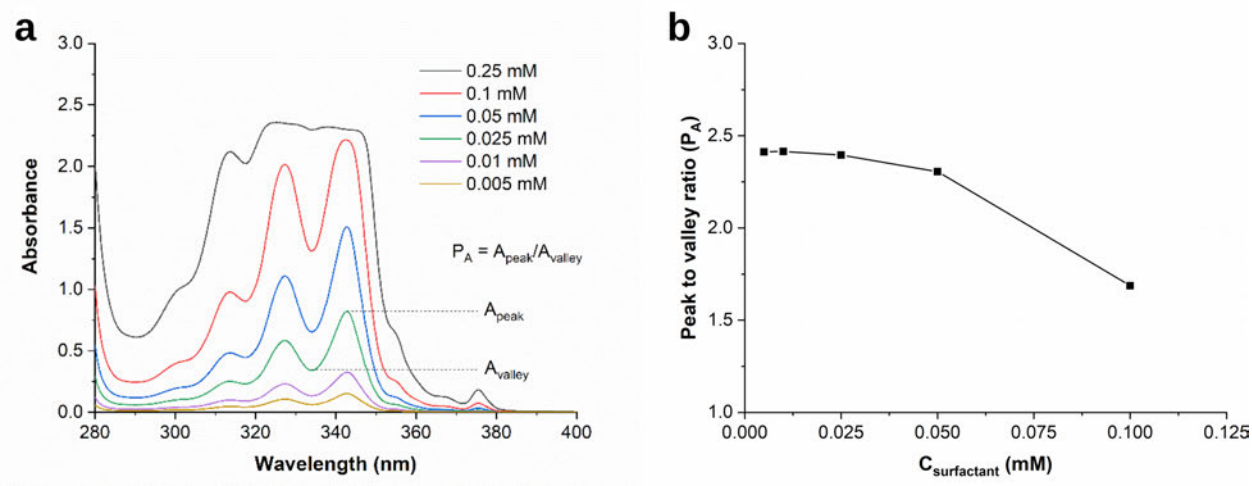

Figure S1: a) UV absorption spectra for surfactant concentrations between 5 μM and 0.25 mM. b) Peak-to-valley ratio (P_A) as a function of surfactant concentration.

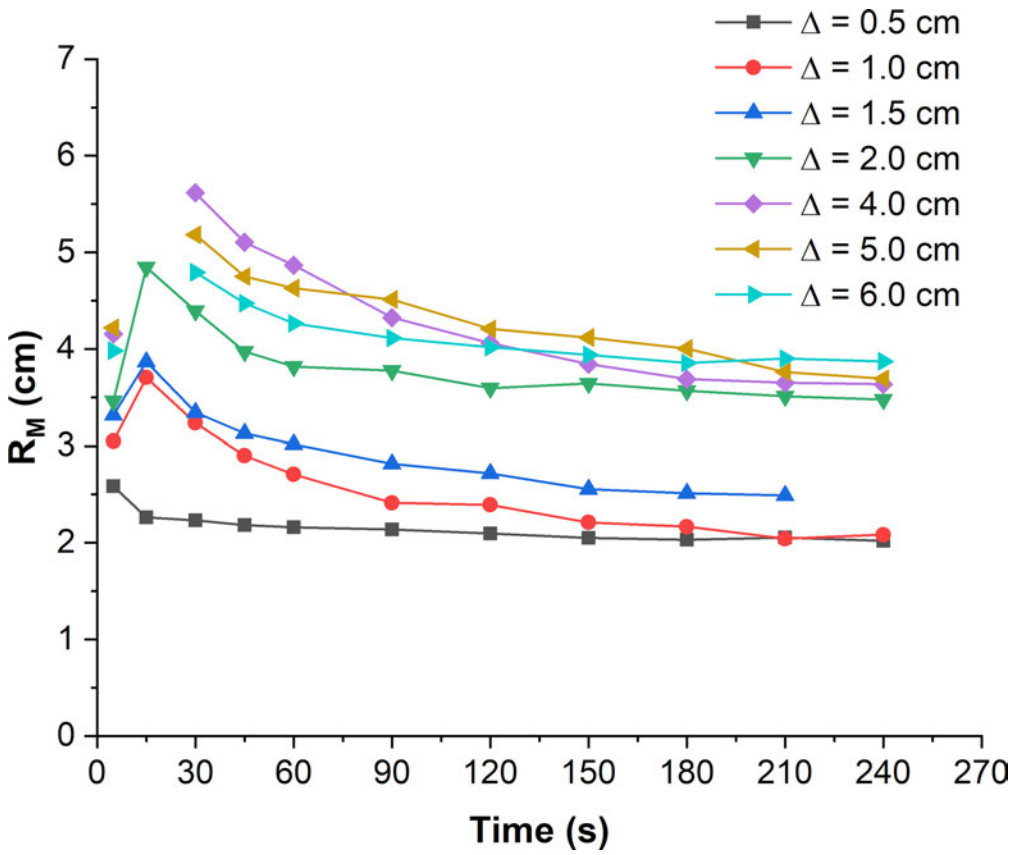

Figure S2: Radius of the Marangoni zone R_M as a function of time for various water depths Δ in a Petri dish. Flow rate is 60 mL.h^{-1}.

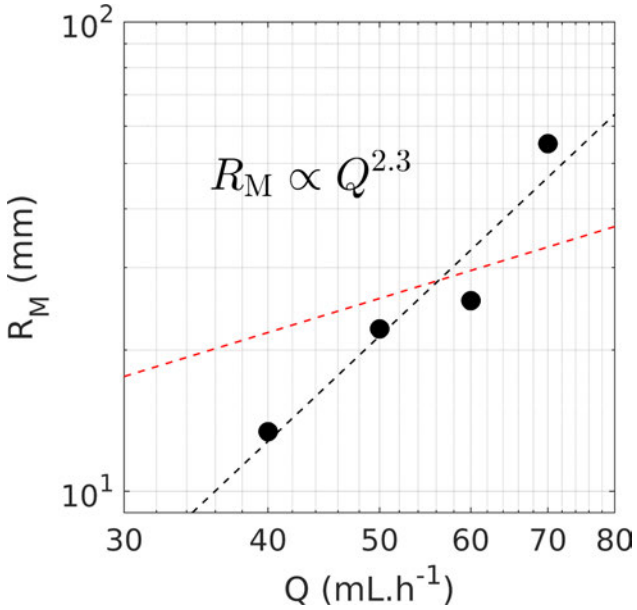

Figure S3: Radius of the Marangoni zone R_{M} measured in a Petri dish 100 s after injection as a function of the flow rate Q. Both axes are in logarithmic scale. The dashed black line is a power law fit showing that R_{M} scales as $Q^{2.3}$, while the dashed red line represents the theoretical variation in $Q^{3/4}$. Water depth is 1.0 cm.

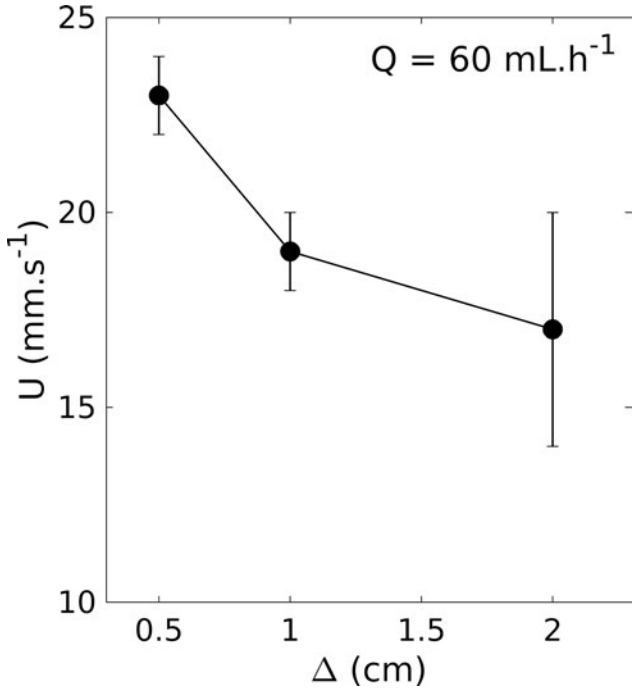

Figure S4: Variations of average velocity U in the Marangoni zone as a function of the water depth Δ at a fixed flow rate of 60 mL.h^{-1}. U is estimated by monitoring the displacement of a polystyrene bead deposited at the water surface, from the injection point to the edge of the Marangoni zone. Measurements are performed in a large tank.

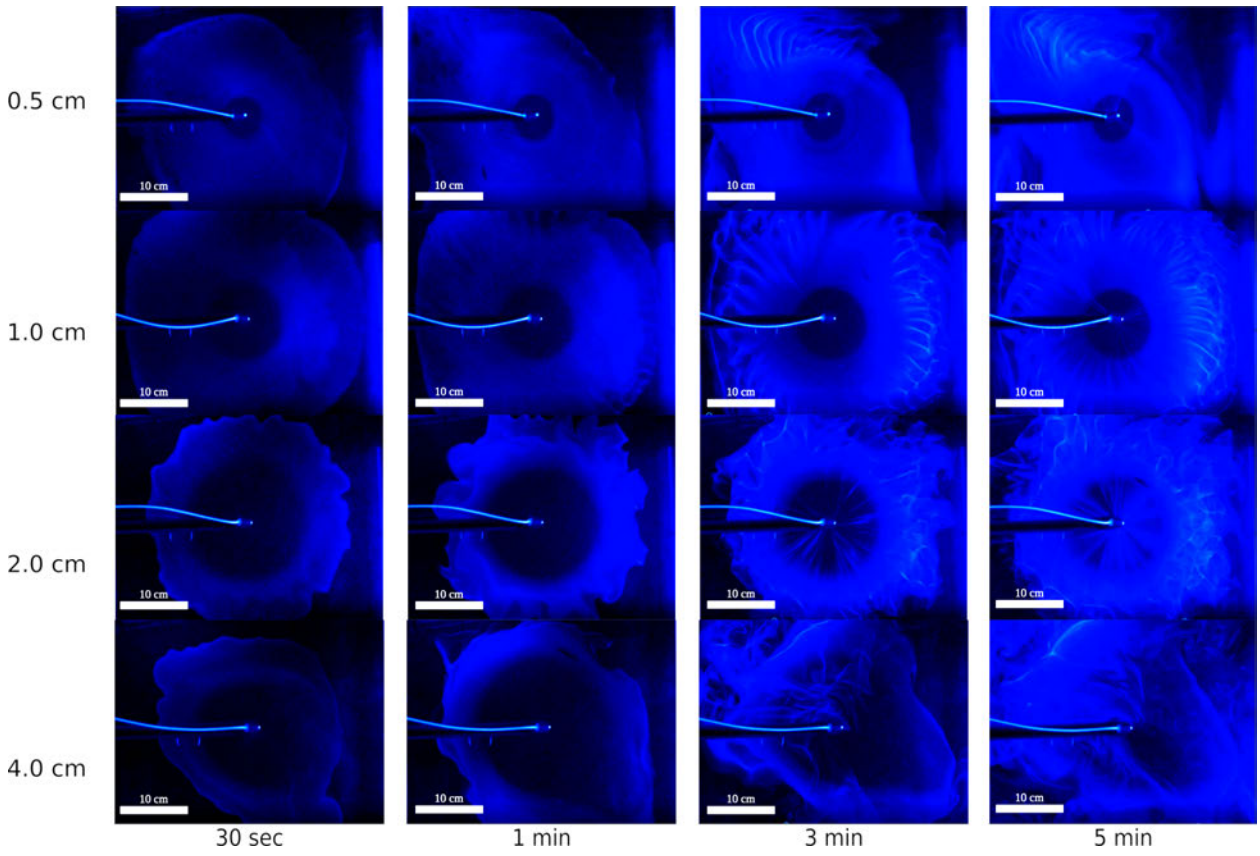

Figure S5: Optical images of fluorescent surfactant flows in experiments performed in a large tank, at various water depths and time steps. Flow rate is 60 mL.h^{-1} in all cases.